

***In Situ* Growth of Bi Nanoparticles on NaBiO₃, and BiO Surfaces: Electron Irradiation and Theoretical Insights**

Marcelo de Assis, Marisa Carvalho de Oliveira, Thales Rafael Machado, Nadia Guerra Macedo, João Paulo de Campos da Costa, Lourdes Gracia, Juan Andrés, and Elson Longo

J. Phys. Chem. C, **Just Accepted Manuscript** • DOI: 10.1021/acs.jpcc.8b11566 • Publication Date (Web): 04 Feb 2019

Downloaded from <http://pubs.acs.org> on February 5, 2019

Just Accepted

“Just Accepted” manuscripts have been peer-reviewed and accepted for publication. They are posted online prior to technical editing, formatting for publication and author proofing. The American Chemical Society provides “Just Accepted” as a service to the research community to expedite the dissemination of scientific material as soon as possible after acceptance. “Just Accepted” manuscripts appear in full in PDF format accompanied by an HTML abstract. “Just Accepted” manuscripts have been fully peer reviewed, but should not be considered the official version of record. They are citable by the Digital Object Identifier (DOI®). “Just Accepted” is an optional service offered to authors. Therefore, the “Just Accepted” Web site may not include all articles that will be published in the journal. After a manuscript is technically edited and formatted, it will be removed from the “Just Accepted” Web site and published as an ASAP article. Note that technical editing may introduce minor changes to the manuscript text and/or graphics which could affect content, and all legal disclaimers and ethical guidelines that apply to the journal pertain. ACS cannot be held responsible for errors or consequences arising from the use of information contained in these “Just Accepted” manuscripts.



***In Situ* Growth of Bi Nanoparticles on NaBiO₃, δ-, and β-Bi₂O₃ Surfaces: Electron Irradiation and Theoretical Insights**

Marcelo Assis ^a, Marisa Carvalho de Oliveira ^b, Thales Rafael Machado^a, Nadia Guerra Macedo^a, João Paulo Campos Costa^a, Lourdes Gracia ^b, Juan Andrés ^{*b} and Elson Longo ^a

^aCDMF, LIEC, Federal University of São Carlos (UFSCar), P.O. Box 676, 13565-905 São Carlos, SP, Brazil

^bDepartment of Analytical and Physical Chemistry, University Jaume I (UJI), Castelló 12071, Spain

Corresponding Author

* E-mail: andres@qfa.uji.es

Phone number: 0034964728083/Fax number: 0034964728066

ABSTRACT: Herein, we present a combined experimental and theoretical study of the *in situ* growth of Bi nanoparticles on NaBiO₃, δ-, and β-Bi₂O₃ surfaces mediated by the electron beam of a high-resolution transmission electron microscope. Density functional theory and quantum theory of atoms in molecules calculations were used to gain a deeper insight into the experimental observations and to provide an atomistic basis for understanding the formation mechanism of Bi NPs on NaBiO₃, δ-, and β-Bi₂O₃ under electron beam irradiation. Analysis of the experimental data and electron density distributions suggests that the formation of Bi NPs can be related to the structural and electronic changes occurring within the octahedral [BiO₆] clusters, and to a lesser extent, [NaO₆] clusters, which serve as the constituent building blocks of NaBiO₃. Our findings indicate that as a function of the number of added electrons, the formation of β-Bi₂O₃ takes place first followed by the subsequent appearance of metallic Bi NPs generated in the crystal by electron beam irradiation.

1. Introduction

The properties derived from the interactions of electrons/waves with matter are of great importance in modern science and engineering. Electron beam irradiation is a necessary and promising area of research because of its wide usage and unique advantages. Furthermore, it is known to be an effective technique for changing or modifying materials; the scattered electrons exiting the back surface of the specimen are a rich source of information about the microstructure and electronic structure of the sample, which can be analyzed based on a variety of electron-solid interaction mechanisms¹⁻³

Conventional techniques for characterizing the microstructure of nanomaterials rely heavily on electron microscopy techniques, in which high-energy electrons are transmitted through the specimen and provide useful information at the nanometer and sub-nanometer levels based on a variety of electron-solid interactions.⁴ The electron beam generated within a transmission electron microscope (TEM) or field emission-TEM (FE-TEM) interacts with the sample during imaging and is also a very powerful tool for the fabrication and manipulation of nanostructures with the advantage of precise control at the nanoscale or single nanoparticle (NP) level.⁵⁻⁶ This is because in a vacuum chamber, despite recent developments in liquid-cell and *in situ* electron microscopy, the high-energy beam used in an electron microscope is unaffected by chemicals in the surrounding environment, such as solvents, reactants, and electrolytes, which can play an essential role in regulating the chemical activity.⁷⁻⁹ TEM can be used to fabricate unique highly dispersed nanomaterials by electron beam irradiation, and Bohler et al.¹⁰ reviewed how low-energy electron irradiation is capable of initiating the synthesis of NPs and modifying surfaces with metal NPs. Very recently, Rummeli et al.¹ reviewed the body of work available on electron-beam-induced synthesis techniques with *in situ* capabilities.

1
2
3 A tremendous amount of research effort has been devoted to the synthesis of metal
4 NPs on the surfaces of different substrates as they may possess innovative properties and
5 hold great promise for future technology.¹¹⁻¹² In particular, arrays of metal NPs deposited on
6 surfaces offer great potential for the design of novel nanomaterials for applications in areas
7 such as catalysis, electronic nanodevices, information storage, and quantum computers.¹³⁻¹⁸
8 Thus, it is crucial to investigate the mechanisms governing the formation and modification
9 of metal NPs during characterization under electron beam irradiation.
10
11
12
13
14
15
16
17
18

19 Our research group have proven that through electron beam irradiation under Ag-
20 based oxides such as α -Ag₂WO₄,¹⁹⁻²⁷ β -Ag₂WO₄,²⁸⁻²⁹ Ag₂CrO₄,³⁰ Ag₂MoO₄,³¹ β -AgVO₃,³²
21 Ag₃PO₄,³³ Ag NPs can be obtained on the surface of these materials. Other metal
22 nanoparticles were also obtained with electron beam irradiation, such as Li,³⁴ Cu,³⁵ Co³⁶ and
23 Au,³⁷ being their formation dependent on the electron beam acceleration voltage, the
24 irradiation time, the nature of the material to be irradiated, among other factors. Even very
25 recently, we have shown the formation and coexistence of different crystallographic phases
26 (rhombohedral, monoclinic, and cubic) of Bi NPs synthesized by femtosecond radiation in
27 air.³⁸ As a continuation of these works, in the current investigation, we demonstrate that an
28 electron beam can be used for the formation of Bi NPs on the surface of NaBiO₃.
29
30
31
32
33
34
35
36
37
38
39
40
41
42

43 Previously, Yacaman et al.³⁹ reported the formation of metallic Bi NPs by focusing a
44 TEM electron beam over NaBiO₃. Very recently, Zhang et al.⁴⁰ observed the formation of Bi
45 NPs by electron irradiation of NaBi(MoO₄)₂ nanosheets at observable conditions (200 kV)
46 in a TEM. While Li et al.⁴¹ managed to unravel the *in situ* atomic-scale mechanism of crystal
47 nucleation and growth of Bi NPs under an electron beam inside an aberration-corrected
48 transmission electron microscope. Electrons interact with solids at the quantum level, and
49
50
51
52
53
54
55
56
57
58
59
60

1
2
3 improving our understanding and predicting the response of a material to the passage of
4 electrons is critical for various applications, but remains a challenging problem. Several
5 questions remain regarding the structural evolution of the crystal lattice during electron
6 irradiation. Bi NPs were also produced by Bi metallic targets in solvents through laser
7 ablation, obtaining spherical nanoparticles of rhombohedral Bi with size range between 60
8 to 5 nm, the size being dependent on the aperture of the laser spot size, the wavelength and
9 laser power, pulse numbers, time slot, solvent employed, among other factors.⁴²⁻⁴⁴

10
11
12 In order to reproduce the experimental scenario as closely as possible, density
13 functional theory (DFT) calculations using the quantum theory of atoms in molecules
14 (QTAIM) were carried out to gain atomistic insights into the *in situ* growth, and structural
15 and electronic evolution of Bi NPs in the NaBiO₃ crystal, as defined by the changes in the
16 electron density. Experimental techniques such as high-resolution transmission electron
17 microscopy (HR-TEM) were used. Energy-dispersive X-ray spectroscopy (EDS) was also
18 employed. The results provide a valuable probe into the relationship between atomic-scale
19 structural and electronic perturbations.

20
21
22 Our manuscript is organized as follows: The employed experimental techniques and
23 theoretical methods used to model the bulk systems are described and then, the results are
24 presented and discussed, and we finally conclude with our main findings and implications
25 for future work.

26 27 28 **2. Methods**

29 30 31 **2.1. Experimental procedures**

32
33
34 Sodium bismuthate (NaBiO₃, 80%, Neon) with a δ -Bi₂O₃ impurity (see in the
35 supporting information, Figure S1) and bismuth (III) oxide (β -Bi₂O₃, 99.999%, Sigma

1
2
3 Aldrich), both commercial reagents, were used for the experiments. A Jem-2100 LaB6 (Jeol)
4 high resolution transmission electron microscope (HR-TEM) with an accelerating voltage of
5 200 kV coupled with an INCA Energy TEM 200 (Oxford) energy dispersive X-ray
6 spectrometer (EDS) was used to irradiate the sample with electrons after depositing small
7 amounts of the powders directly onto carbon-coated Cu grids, while pellets were prepared
8 by ultrasonic dispersion. In addition, we used the same equipment for performing TEM and
9 microanalysis measurements in order to characterize the structural changes of the samples.
10
11 The mesh size of TEM grids is 300.
12
13
14
15
16
17
18
19
20
21
22
23

24 **2.2. Theoretical methods**

25
26 First-principles total energy calculations were carried out within the periodic DFT
27 framework using the VASP program.⁴⁵ The Kohn-Sham equations were solved by means of
28 the Perdew, Burke, and Ernzerhof exchange-correlation functional, and the electron-ion
29 interaction described by the projector-augmented-wave pseudopotentials.⁴⁶⁻⁴⁷ Because of the
30 well-known limitations of standard DFT in describing the electronic structures of “strongly-
31 correlated” compounds, a correction to the PBE wave function was made (PBE+U) by
32 including a repulsive on-site Coulomb interaction, U, according to the formula of Dudarev
33 et al.⁴⁸ The orbital dependence of the Coulomb and exchange interactions has been taken into
34 account with this scheme, using a value of 6 eV for the Hubbard parameter for Bi (previously
35 tested). The plane-wave expansion was truncated at a cut-off energy of 520 eV and the
36 Brillouin zones were sampled through Monkhorst-Pack special k- point grids that ensured
37 geometrical and energetic convergence for the NaBiO₃, β-Bi₂O₃, and δ-Bi₂O₃ structures
38 considered in this work. In the calculations, electrons were introduced one by one up to eight
39 in the unit cell (keyword NELECT) and the distribution of these extra electrons takes place
40
41
42
43
44
45
46
47
48
49
50
51
52
53
54
55
56
57
58
59
60

1
2
3 by means of a simultaneous geometry optimization on both the lattice parameters and the
4 atomic positions. The relationship between charge density topology and elements of
5 molecular structure and bonding was noted by Bader.⁴⁹ This relationship, Bader's QTAIM
6 theory,⁵⁰⁻⁵¹ is now a well-recognized tool for analyzing electron density, describing
7 interatomic interactions, and rationalizing chemical bonding, as used in previous works.^{23, 26,}
8
9
10
11
12
13
14 28, 30, 32-33, 52-53
15
16
17
18

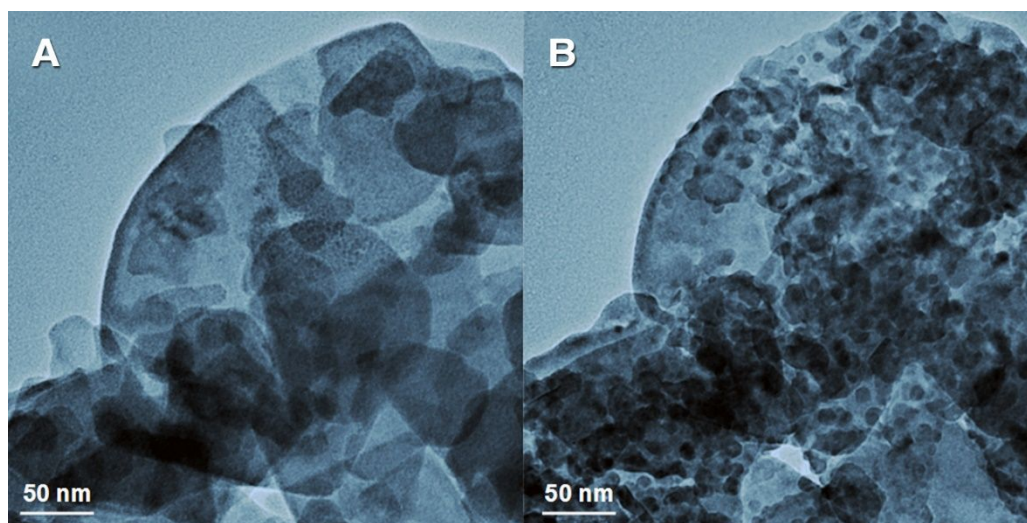
19 **3. Results and discussion**

20
21 The unit cell of NaBiO₃ in the ilmenite structure belongs to the space group R-3. The
22 optimized lattice constants are $a = b = 5.508 \text{ \AA}$, $c = 15.818 \text{ \AA}$, $\alpha = \beta = 90^\circ$, and $\gamma = 120^\circ$,
23 according to other theoretical and experimental works.⁵⁴⁻⁵⁵ There is one type of Na and one
24 type of Bi in a NaBiO₃ crystal, forming both distorted octahedral clusters (see the supporting
25 information file, Figure S2). Both [NaO₆] and [BiO₆] octahedral clusters are distorted with
26 two different bond lengths, where the Na–O bond lengths are longer than the Bi–O bond
27 lengths. Two phases of bismuth oxide (Bi₂O₃) were modeled, β -Bi₂O₃ and δ -Bi₂O₃
28 polymorphs. β -Bi₂O₃ presents a tetragonal structure belonging to the space group P42c
29 (ICSD 62979) and δ -Bi₂O₃ has a cubic structure belonging to the space group Fm $\bar{3}$ m, which
30 was modeled taking into account an occupancy factor of only 0.75 in the 8c Wyckoff
31 positions for the O atoms (ICSD 27458).
32
33
34
35
36
37
38
39
40
41
42
43
44
45

46
47 NaBiO₃ was characterized by X-ray diffraction (XRD) and the corresponding patterns
48 are associated with a hexagonal structure with two hydration molecules (NaBiO₃·2H₂O), as
49 described by PDF 30-1161⁵⁶ in the Joint Committee on Powder Diffraction Standards
50 (JCPDS) database (see supporting information, Figure S1). NaBiO₃ crystals have a
51 hexagonal structure belonging to the space group P3 with two molecular formula units per
52
53
54
55
56
57
58
59
60

1
2
3 unit cell ($Z=2$). Due to its low purity (80%), the δ - Bi_2O_3 phase was also present, according to
4 PDF 52-1007⁵⁷ in the JCPDS database. These results can be attributed to the fact that
5
6
7
8 $\text{NaBiO}_3 \cdot 2\text{H}_2\text{O}$ is obtained at high temperatures through the oxidation of $\text{Bi}(\text{NO}_3)_3 \cdot 5\text{H}_2\text{O}$ by
9
10 NaOH ,⁵⁸ and therefore, the hexagonal polymorph of NaBiO_3 and cubic polymorph of δ - Bi_2O_3
11
12 are obtained.
13

14
15 NaBiO_3 was irradiated using an electron beam under high *vacuum* in a TEM at 200
16
17 kV. Figure 1 shows low-magnification TEM images of the material before being irradiated.
18
19 According to Figure 1B, after 10 minutes of irradiation with the electron beam, the formation
20
21 of nanocrystals of Bi could be observed on the surface of the sample.
22
23
24
25
26
27



45
46 **Figure 1:** (A) Low-magnification TEM image of the sample before the irradiation by electron
47 beam and (B) after 10 minutes of exposure to irradiation by electron beam.
48
49
50

51
52 The effect of exposure time was investigated and the TEM images are displayed in
53
54 Figures 2A-B and 2D-E. An analysis of the results suggests that the morphology of the Bi
55
56
57
58
59
60

1
2
3 NPs changes with time with the formation of agglomerates with non-regular shapes and
4 diameters of about 10-100 nm. In Figure 1B it is also possible to observe spheroidal NPs and
5
6
7 some particles with morphology of beans or earthworms, like in figure 2A, which could be
8
9 associated to the irregular shape of the initial particles or coalescence of some spheroidal NPs
10
11 as an effect of electron beam irradiation. It can be observed that as the electron irradiation
12
13
14 time increases, the Bi NPs perform a coalescence process to form larger particles. At short
15
16 times of electron irradiation, the formation of NPs of Bi is more slowly, while at lower
17
18 acceleration voltages (5-30 kV that are obtained in SEM), it is observed that the energy of
19
20 the electron beam is not enough to provoke the reduction of Bi, being this process dependent
21
22 on the energy of the electron beam.
23
24
25

26
27 Semi-quantitative analysis of the EDS data shows that, at first, we have very similar
28
29 amounts of Na and Bi, due to the stoichiometry of the compound. Because δ -Bi₂O₃ is an
30
31 impurity present in the NaBiO₃, a slightly higher amount of Bi was observed at the start of
32
33 experiments (Figure 2C). After the formation of the agglomerates on the surface of the
34
35 material and its subsequent degradation, an increase in the amount of Bi (91%) was observed
36
37 due to the reduction of Bi (V) to metallic Bi (Figure 2F). The Cu and C elements observed
38
39 in the EDS data are from the sample port. A similar behavior was found by Zheng et al.⁵⁹ in
40
41 their study of the *in situ* coalescence process of Bi NPs by liquid cell TEM.
42
43
44
45
46
47
48
49
50
51
52
53
54
55
56
57
58
59
60

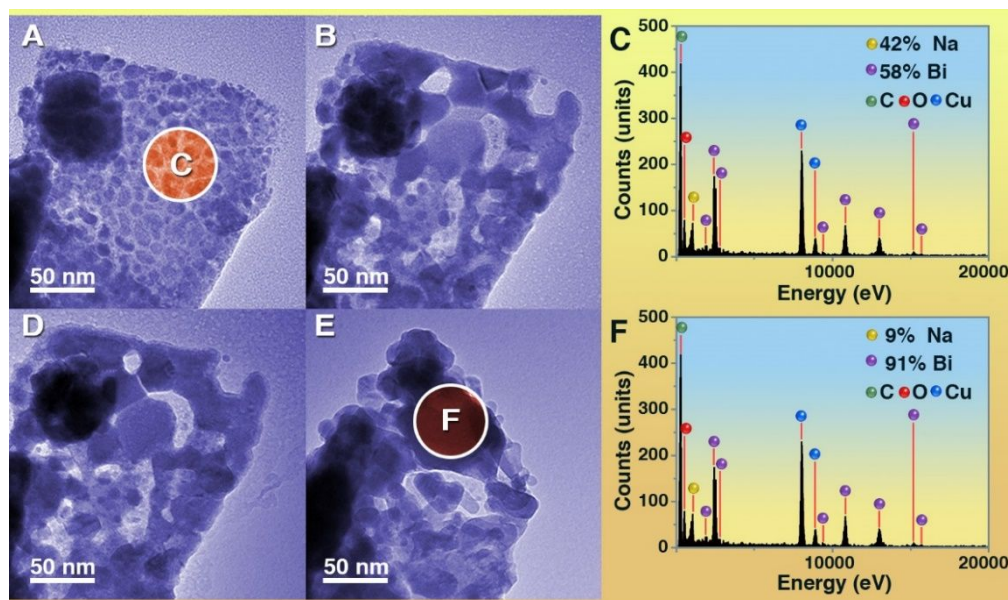


Figure 2: TEM image of the sample after (A) 10, (B) 15, (D) 20 and (E) 30 minutes of exposure. (C) and (F) EDS of the white circle in the image and their quantification.

High-resolution micrographs (HR-TEM) were taken to analyze the formed nanocrystals (Figure 3). Before irradiation with the electron beam, the (110) plane with an interplanar distance of 2.80 Å (Figure 3B) characteristic of hexagonal NaBiO_3 ⁵⁶ was found, and EDS analysis was performed to confirm the presence Na in the material (see supporting information, Figure S3). After 10 minutes of exposure (Figures 3C-D), small crystalline non-regular clusters appeared, and they were analyzed. The (012) plane with an interplanar distance of 3.28 Å was observed, corresponding to the rhombohedral structure of metallic Bi (Figures E-G) associated with PDF 44-1246⁶⁰ in the JCPDS database.

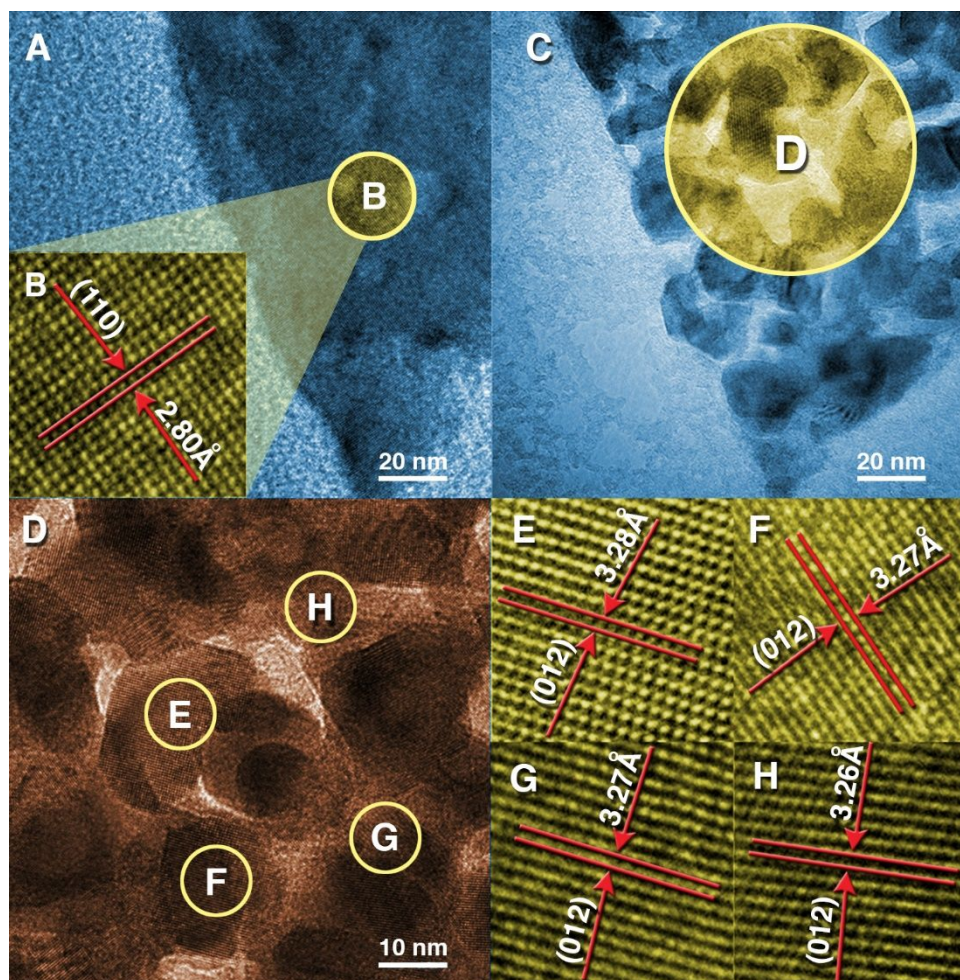


Figure 3 - TEM image of the NaBiO₃ before (A-B) the irradiation by electron beam and after (C). (D) HR-TEM micrographs at higher magnification (C). (E), (F), (G) and (H) NPs of Bi rhombohedral.

Under electron beam irradiation, there is a redistribution of electrons, associated with transitions of electrons from occupied to unoccupied states in the band structure of the crystal. The occupied states in the valence band, VB, are below the Fermi level (quantum stable) and the unoccupied states in the conduction band, CB, are mostly above the Fermi level (unstable states, i.e. quantum excited states). These rearrangements induce oxidation-reduction

1
2
3 reactions, and in the present case, the octahedral [BiO₆] cluster of NaBiO₃ accumulates an
4
5 excess of electron density, producing a continuous reduction in the oxidation state of Bi from
6
7 (V) to zero (metallic Bi), via Bi (III) in Bi₂O₃.
8
9

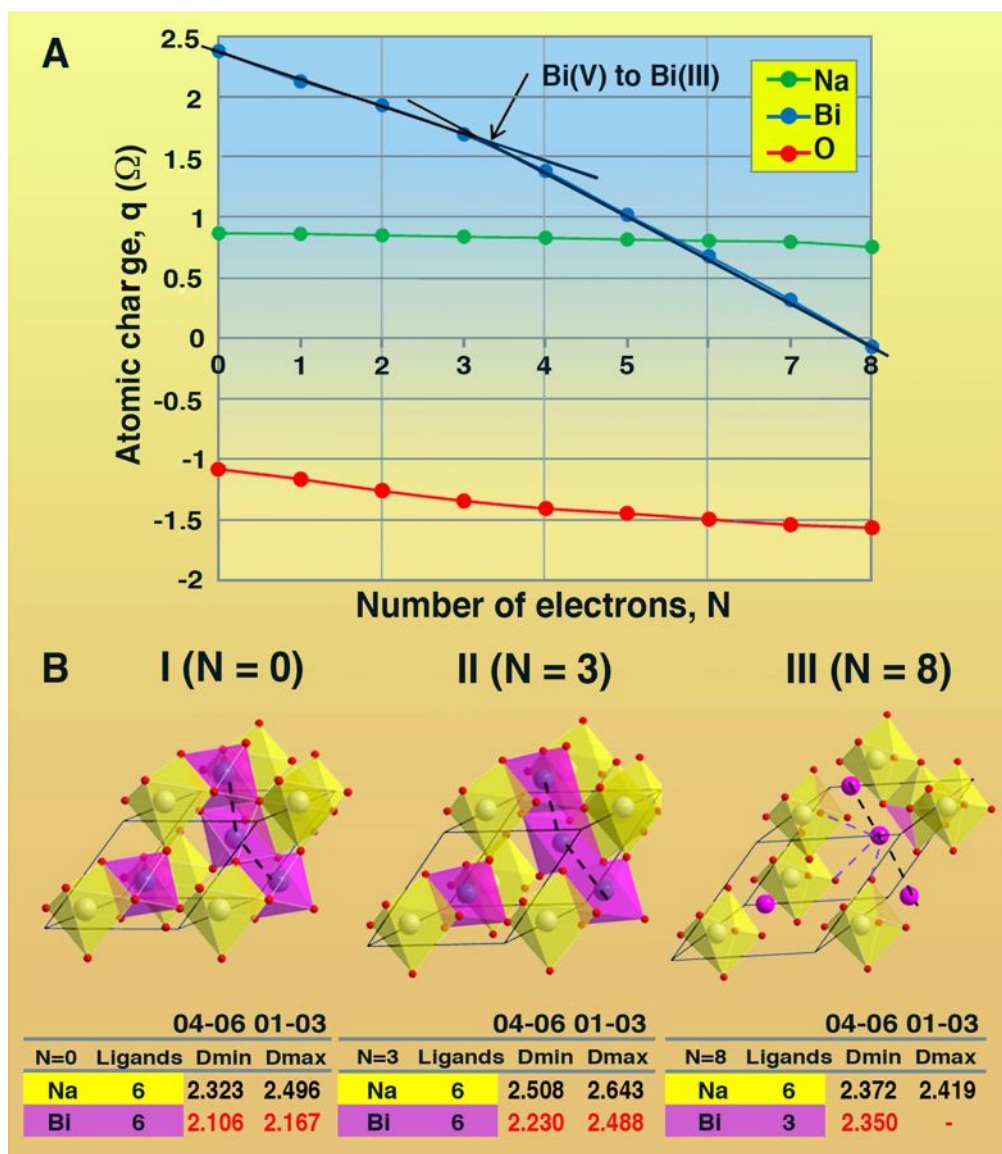
10 NaBiO₃ is an n-type semiconductor. After the electron beam irradiation, the Bi-rich
11
12 region becomes an n/p-type semiconductor due to the formation of internal defects caused
13
14 by Bi vacancies in localized areas, thus enhancing the transfer and separation of photo-
15
16 generated electron-hole pairs. Then, the action of the electron beam of the TEM induces the
17
18 reduction of Bi cations in NaBiO₃ and the subsequent segregation of metallic Bi through the
19
20 NaBiO₃ crystalline lattice. This creates regions with Bi vacancies (V_{Bi}) which function as an
21
22 n-type semiconductor, and regions with oxygen vacancies (V_O), which function as a p-type
23
24 semiconductor. The formation of this p-n junction between the xBi/NaBi_{1-x}O₃ heterostructure
25
26 is expected to enhance the reduction activity by enhancing the conductivity, electron
27
28 mobility, and lifetime of photo-generated electron-hole pairs.
29
30
31
32

33 A comparison with the results obtained in our previous paper which Bi NPs are
34
35 obtained by femtosecond laser,³⁸ renders that the large number of photons generated in a
36
37 femtosecond laser interacts with NaBiO₃ substrate, is capable to produce a plasma with high
38
39 pressure and temperature values (10¹⁰–10⁹ Pa and 1000 K, respectively). These critical
40
41 conditions allow the three distinct phases of Bi to coexist: rhombohedral, cubic and tetrahedral.
42
43 Hence, the present results demonstrate that the experimental conditions from the synthesis
44
45 using an electron beam of TEM *in vacuum* can selectively produce the most stable
46
47 rhombohedral structure of metallic Bi. This experimental observation is also consistent with
48
49 the literature reporting the formation metallic Bi in a TEM.³⁹
50
51
52
53

54 To gain a deeper insight into these experimental observations and to provide some
55
56 basis upon which to understand the effects described above, a detailed theoretical study of
57
58
59
60

1
2
3 the electronic charge of each atom was conducted using Bader charge analysis within the
4 QTAIM framework. Finding zero flux surfaces between two atoms allows the atomic charge
5 to be calculated by integrating the charge density within the atomic basins, Ω , and subtracting
6 the nuclear charge, Z , of the corresponding atom. The charge densities of the Na, Bi, and O
7 centers as a function of the number of electrons added are depicted in Figure 4A and the
8 values are collected in Table S1 of the supporting information. In addition, the primitive cell
9 of NaBiO_3 without and with the addition of 3 and 8 electrons and the distances from their
10 metallic centers to the corresponding oxygen atoms, i.e., the Na-O and Bi-O bond lengths,
11 are presented in Figure 4B. An analysis of Figure 4A shows that the charge density of the Na
12 centers is maintained, whereas the Bi centers of the $[\text{BiO}_6]$ clusters show decreasing charge
13 densities with different behavior as electrons are added. From the addition of 3 electrons
14 onward, the decrease in the Bi charge density becomes more noticeable.

15
16
17
18
19
20
21
22
23
24
25
26
27
28
29
30
31 At the same time, the two Bi-O distances start to change after the addition of 3
32 electrons, as can be seen in Figure SI-4 of the supporting information. The pronounced
33 decrease in Bi charge density continues upon increasing N from 4 to 8, in which range only
34 three Bi-O distances were found. It is interesting to note that for the $[\text{NaO}_6]$ octahedral
35 clusters, the two Na-O distances remain almost unaltered. These findings suggest a possible
36 decomposition of NaBiO_3 into Bi_2O_3 , and then the continued reduction of Bi (III) to metallic
37 Bi.
38
39
40
41
42
43
44
45
46
47
48
49
50
51
52
53
54
55
56
57
58
59
60



40 **Figure 4** - (A) Bader charge density of Bi, Na and O centers as a function of the number of
41 electrons added. $q(\Omega)$ represents the number of valence electrons minus the calculated charge
42 density; (B) Primitive cell without (I) and with the addition of 3 (II) and 8 electrons (III) in
43 NaBiO₃ and the minimum and maximum distances in Å (d_{\min} and d_{\max} , respectively) of the
44 metallic centers to their oxygen atoms.

45
46
47 In Figure 5 the variation of the positions of both VB and CB is analyzed along the process
48 of addition of electrons. First, in the neutral NaBiO₃ system ($N=0$), with the addition of three
49
50
51
52
53
54
55
56
57
58
59
60

(N=3) and eight (N=8) electrons in order to visualize the reduction in the oxidation state of Bi from (V) to Bi (III) in Bi_2O_3 and to metallic Bi (zero), respectively. This scheme showed in Figure 5 follows the common case of a heterojunction based on the n-type semiconductor and metal, in which at the interface of the materials electrons flow from the semiconductor into the metal to adjust the Fermi energy levels.

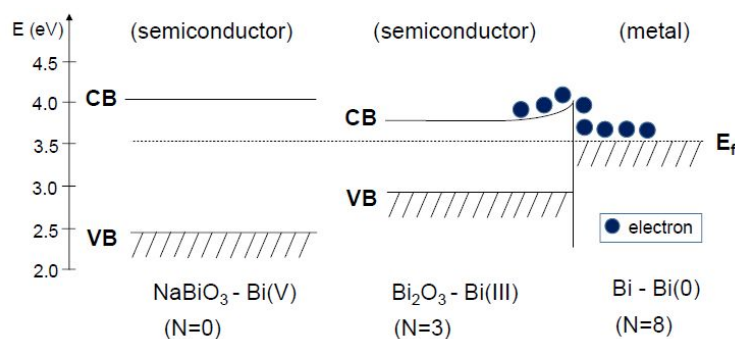


Figure 5 - Variation of the positions of VB and CB as a function of the number of electrons added, N. The position of the Fermi energy level, E_f , is placed once the metallic Bi is formed.

Bader charge analysis for the tetragonal $\beta\text{-Bi}_2\text{O}_3$ and cubic $\delta\text{-Bi}_2\text{O}_3$ structures was performed and the results are presented in Figures 6 and 7, respectively. The charge densities of the Bi and O centers as a function of the number of electrons added to $\beta\text{-Bi}_2\text{O}_3$ are depicted in Figure 6A, while its unit cell without and with the addition of 6 and 15 electrons and the distance between its metallic centers to the corresponding oxygen anions are presented in Figure 6B. An analysis of the results suggests that the Bi centers of the $[\text{BiO}_5]$ clusters decrease their charge density gradually up to 6 electrons added, at which point the Bi coordination number changes and is reduced to three. After the addition of 6 electrons, the coordination was maintained while the Bi-O distance increased up to 2.531 Å for N=15, where the Bi atom was completely reduced (Figure S5). The charge density of the Bi and O

centers as a function of the number of electrons added to δ - Bi_2O_3 is presented in Figure 7A, while its cubic unit cell without and with the addition of 8 electrons is shown in Figure 7B. Bi centers of the cabin-type $[\text{BiO}_6]$ clusters showed gradually decreasing charge densities up to the addition of 8 electrons, at which point the Bi atom was completely reduced, keeping the Bi coordination. At this point, the Bi-O distance increased from 2.394 Å to 2.842 Å due to the cell expansion (Figure S5). The charge density values of Na, Bi and O centers for β - Bi_2O_3 and δ - Bi_2O_3 structures are collected in Table S2 of the supporting information.

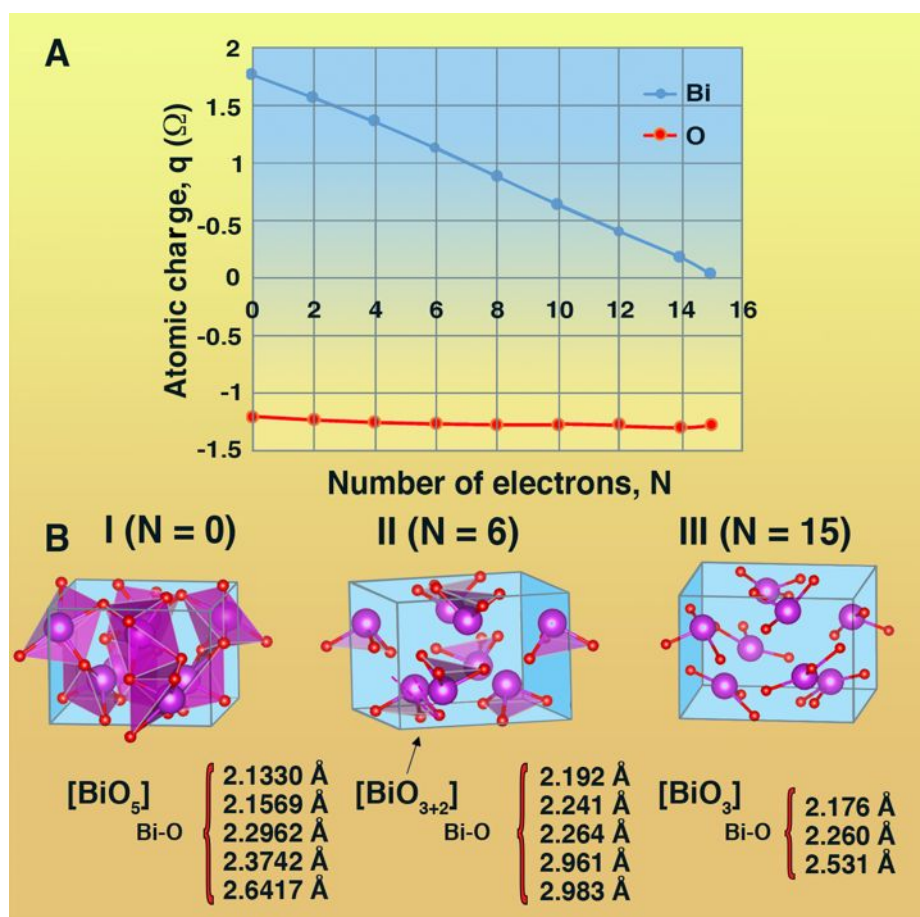


Figure 6 - (A) Bader charge density of Bi and O centers as a function of the number of electrons added. (B) Unit cell β - Bi_2O_3 without (I), with the addition of 6 electrons (II) and with the addition of 15 electrons (III); and the Bi-O distances of the structural clusters.

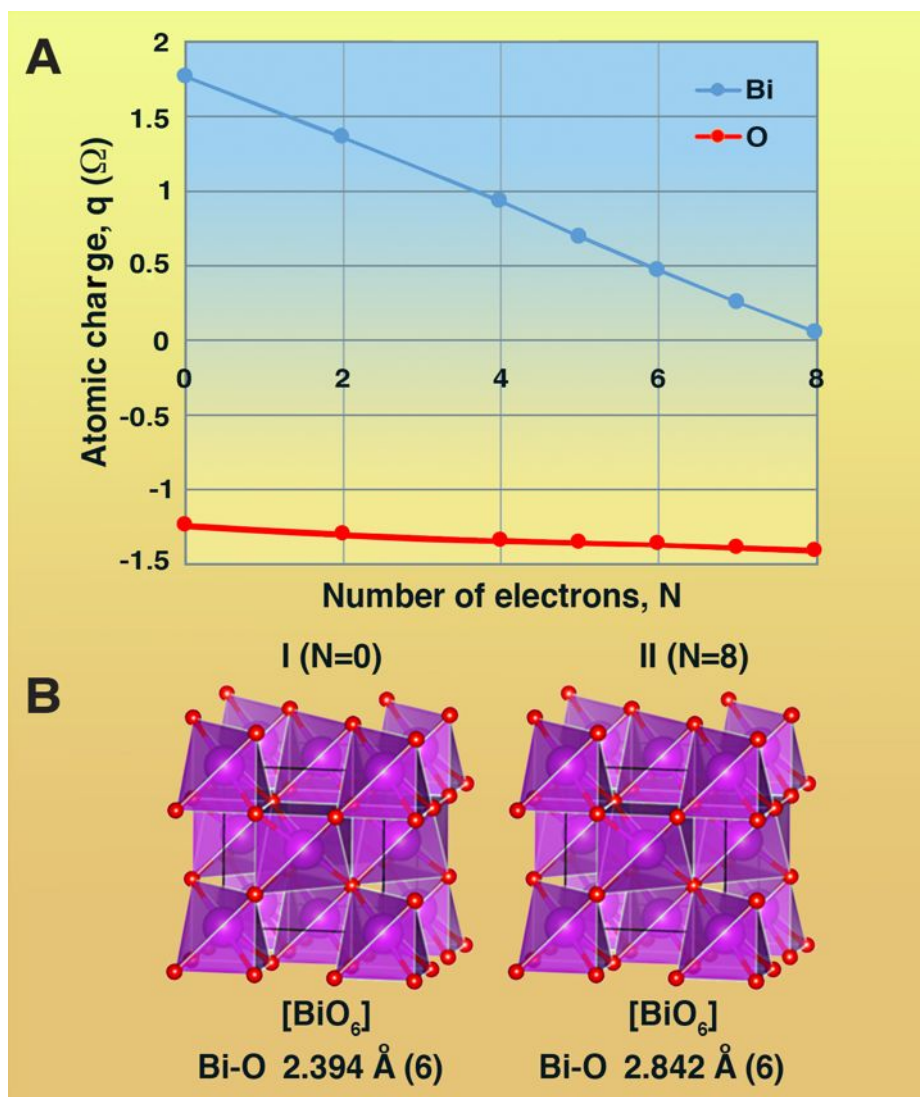


Figure 7 - (A) Bader charge density of Bi and O centers as a function of the number of electrons added. (B) Unit cell δ - Bi_2O_3 without (I) and with the addition of 8 electrons (II); and the Bi-O distances of the structural clusters.

As the transition from Bi (III) to metallic Bi was not observed during the reduction of NaBiO_3 , the same study was performed using β - Bi_2O_3 as the starting reagent (Figure 8). The sample was taken to the TEM and exposed to the electron beam. After 15 minutes of exposure, crystalline clusters started to appear on the surface of the β - Bi_2O_3 , as seen in

1
2
3 NaBiO₃. These NPs were characterized as rhombohedral metallic Bi based on observation of
4 the (012) plane with an interplanar distance of 3.28 Å (Figure 8B), similar to the results
5 obtained for NaBiO₃. The EDS analysis showed that the NPs that appeared on the surface
6 were formed of Bi (99 %), proving that β-Bi₂O₃ undergoes the process of reduction from Bi
7 (III) to metallic Bi (Figure 8C).
8
9
10
11
12
13
14
15
16
17
18
19
20
21
22
23
24
25
26
27
28
29
30
31
32
33
34
35
36
37
38
39
40
41
42
43
44
45
46
47
48
49
50
51
52
53
54
55
56
57
58
59
60

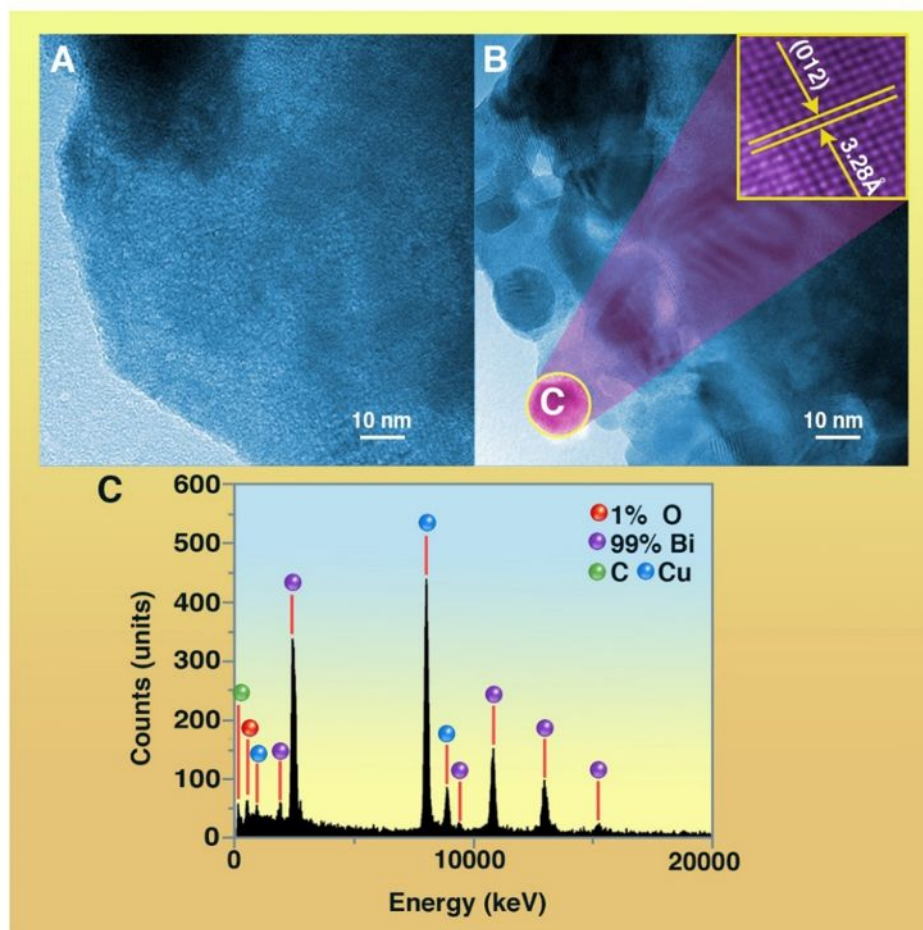


Figure 8 - (A) TEM image of the β-Bi₂O₃ before the irradiation by electron beam and (B) after 15 minutes exposure. (C) EDS of the yellow circle in the image and their quantification.

4. Conclusions

During the process of TEM observation (interaction of an electron beam with matter), some novel phenomena were discovered. These interactions can be used to fabricate NPs and investigate their structure and chemical transformation, which is of importance for the development of novel nanostructures, especially for those that cannot be obtained using conventional chemical and physical methods.

In this work, we studied the in situ crystal growth of pure single crystals of metallic Bi on the surface of NaBiO_3 , $\delta\text{-Bi}_2\text{O}_3$, and $\beta\text{-Bi}_2\text{O}_3$ under the electron beam of an FE-TEM. First principles calculations at the DFT level and QTAIM analysis were combined with different characterization techniques, including HR-TEM and EDS to extend our fundamental understanding of the atomic processes that underpin the formation of Bi NPs on these materials mediated by electron beam irradiation.

The main conclusions of the present work can be summarized as follows: i) Both theoretical and experimental findings can be used to find a relationship between atomic-scale structural and electronic perturbations induced by electron beam irradiation, providing adequate conditions for the formation of Bi NPs on NaBiO_3 ; ii) Electron beam irradiation can induce the breaking of Bi-O, and to a lesser extent Na-O, bonds in the $[\text{BiO}_6]$ and $[\text{NaO}_6]$ clusters, respectively, as constituent building blocks of NaBiO_3 ; iii) Under electron beam irradiation, a redistribution of electrons takes place with a concomitant reduction in the oxidation state of Bi from (V) to zero (metallic Bi); iv) First, the formation of $\beta\text{-Bi}_2\text{O}_3$, with a Bi (III) oxidation state, takes place followed by the subsequent appearance of metallic Bi NPs; v) These structural and electronic perturbations of the material provoke a change from n-type to p-type semiconductor behavior associated to the formation of a p-n $x\text{Bi}/\text{NaBi}_{1-x}\text{O}_3$ heterostructure.

1
2
3 With the use of robust experimental and theoretical tools, scientists now have the
4 capability to push the limits of investigation to the ultimate level of individual atoms and
5 single bonds. If this knowledge can be transformed to develop useful NPs, then exciting
6 opportunities to engineer novel assemblies for new applications are wide open. The current
7 work sheds light on the potential use of electron beams to trigger the formation of Bi and
8 other metal NPs.
9
10
11
12
13
14
15
16
17
18

19 **Acknowledgments**

20
21 The authors acknowledge the financial support of agencies: Coordenação de
22 Aperfeiçoamento de Pessoal de Nível Superior – Brazil (CAPES) – Finance code 001 –
23 PNPB program, FINEP, FAPESP (2013/07296-2, 2013/26671-9), CNPq (166281/2017-4),
24 Generalitat Valenciana for PrometeoII/2014/022, ACOMP/2015/1202, Ministerio de
25 Economia y Competitividad, project CTQ2015-65207-P, and Universitat Jaume I” project
26 No. UJI-B2016-25. The authors thanks to Enio Longo for the support with the scientific
27 illustrations. The authors also thank the Servei d’Informàtica, Universitat Jaume I, for
28 generous allocation of computer time.
29
30
31
32
33
34
35
36
37
38
39
40
41
42
43

44 **Supporting Information**

- 45
46 - XRD patterns for commercial NaBiO₃
47
48 - Conventional and primitive cell of NaBiO₃ in the rhombohedral space group R-3
49
50 - EDS analysis of NaBiO₃
51
52 - Variation of Bi-O distances and of cell parameters in NaBiO₃ structure as a
53 function of the number of electrons added, N
54
55
56
57
58
59
60

- 1
2
3 - Variation of cell parameters in Bi_2O_3 structure as a function of the number of
4 electrons added, N. (A) $\beta\text{-Bi}_2\text{O}_3$ and (B) $\delta\text{-Bi}_2\text{O}_3$
5
6
7
8
9
10

11 **References**

- 12
13
14 (1) Gonzalez-Martinez, I. G.; Bachmatiuk, A.; Bezugly, V.; Kunstmann, J.; Gemming, T.,
15 Liu, Z.; Cuniberti, G.; Rümelli, M. H. Electron-Beam Induced Synthesis of Nanostructures:
16 A Review. *Nanoscale* **2016**, *08*, 11340-11362.
17
18
19
20
21
22
23 (2) Zhang, W.; Zheng, W. T. Transmission Electron Microscopy Finds Plenty of Room on
24 the Surface. *Phys. Chem. Chem. Phys.* **2015**, *17*, 14461-14469.
25
26
27
28
29
30 (3) Williams, D. B.; Carter, C. B. *Transmission Electron Microscopy: a Textbook for*
31 *Materials Science*; Springer: New York, 2009.
32
33
34
35
36
37 (4) Xu, Y.; Shi, L.; Zhang, X.; Wong, K.; Li, Q. The Electron Beam Irradiation Damage on
38 Nanomaterials Synthesized by Hydrothermal and Thermal Evaporation Methods—An
39 Example of ZnS Nanostructures. *Micron* **2011**, *42*, 290-298.
40
41
42
43
44
45
46 (5) Yen, M.-Y.; Chiu, C.-W.; Chen, F.-R.; Kai, J.-J.; Lee, C.-Y.; Chiu, H.-T. Convergent
47 Electron Beam Induced Growth of Copper Nanostructures: Evidence of the Importance of a
48 Soft Template. *Langmuir*, **2004**, *20*, 279-281.
49
50
51
52
53
54
55
56
57
58
59
60

- 1
2
3 (6) Tham, D.; Nam, C.-Y.; Fischer, J. E. Microstructure and Composition of Focused-Ion-
4 Beam-Deposited Pt Contacts to GaN Nanowires. *Adv. Mater.* **2006**, *18*, 290-294.
5
6
7
8
9
10 (7) Liao, H.-G.; Niu, K.; Zheng, H. Observation of Growth of Metal Nanoparticles. *Chem.*
11
12 *Commun.* **2013**, *49*, 11720-11727.
13
14
15
16
17 (8) Moser, T. H.; Mehta, H.; Park, C.; Kelly, R.T.; Shokuhfar, T.; Evans, J. E. The Role of
18 Electron Irradiation History in Liquid Cell Transmission Electron Microscopy. *Sci. Adv.*,
19 **2018**, *4*, eaaq 1202.
20
21
22
23
24
25
26 (9) Mirsaidov, U. M.; Zheng, H.; Bhattacharya, D.; Casana, Y.; Matsudaria, P. Direct
27 Observation of Stick-slip Movements of Water Nanodroplets Induced by an Electron Beam.
28 *Proc. Natl. Acad. Sci.*, **2012**, *109*, 7187-7190.
29
30
31
32
33
34
35 (10) Böhler, E.; Warneke, J.; Swiderek, P. Control of Chemical Reactions and Synthesis by
36 Low-energy Electrons. *Chem. Soc. Rev.* **2013**, *42*, 9219-9231.
37
38
39
40
41
42 (11) Su, Q.; Li, J.; Zhong, G.; Du, G.; Xu, B. In Situ Synthesis of Iron/Nickel Sulfide
43 Nanostructures-Filed Carbon Nanotubes and Their Electromagnetic and Microwave-
44 Absorbing Properties. *J. Phys. Chem. C* **2011**, *115*, 1838-1842.
45
46
47
48
49
50
51 (12) Hu, J.; Sun, Y.; Chen, Z. Rapid Fabrication of Nanocrystals Through In Situ Electron
52 Beam Irradiation in a Transmission Electron Microscope. *J. Phys. Chem. C*, **2009**, *113*,
53 5201-5205.
54
55
56
57
58
59
60

1
2
3
4
5 (13) Zhu, Y. T.; Liao, X. Nanostructured Metals: Retaining Ductility. *Nat. Mater.*, **2004**, *3*,
6 351-352.
7
8

9
10
11 (14) Lee, J. S.; Kovalenko, M. V.; Huang, J.; Chung, D. S.; Talapin, D.V. Band-like
12 Transport, High Electron Mobility and High Photoconductivity in All-Inorganic Nanocrystal
13 Arrays. *Nat. Nanotechnol.*, **2011**, *6*, 348-352.
14
15
16
17
18

19
20 (15) Yamada, Y.; Tsung, C.-K.; Huang, W.; Huo, Z.; Habas, S. E.; Soejima, T.; Aliaga, C.
21 E.; Somorjai, G.A.; Yang, P. Nanocrystal Bilayer for Tandem Catalysis. *Nat. Chem.* **2011**, *3*,
22 372-376.
23
24
25
26
27

28
29 (16) Lim, D.-W.; Yoon, J. W.; Ryu, K. Y.; Suh, M. P. Magnesium Nanocrystals Embedded
30 in a Metal-Organic Framework: Hybrid Hydrogen Storage with Synergistic Effect on Physi-
31 and Chemisorption. *Angew. Chem. Int.Ed.* **2012**, *51*, 9814-9817.
32
33
34
35
36

37
38 (17) Wu, P.; Yan, X. P. Doped Quantum Dots for Chemo/Biosensing and Bioimaging.
39 *Chem.Soc.Rev.* **2013**, *42*, 5489-521.
40
41
42
43
44

45
46 (18) Cargnello, M.; Doan-Nguyen, V. V. T.; Gordon, T. R.; Diaz, R. E.; Stach, E. A.; Gorte,
47 R. J.; Fornasiero, P.; Murray, C. B. Control of Metal Nanocrystal Size Reveals Metal-Support
48 Interface Role for Ceria Catalysts. *Science* **2013**, *341*, 771-773.
49
50
51
52
53

1
2
3 (19) Longo, V. M.; De Foggi, C. C.; Ferrer, M. M.; Gouveia, A. F.; Andre, R. S.; Avansi,
4 W.; Vergani, C. E.; Machado, A. L.; Andres, J.; Cavalcante, L. S.; et al. Potentiated Electron
5 Transference in Alpha-Ag₂WO₄ Microcrystals with Ag Nanofilaments as Microbial Agent.
6
7
8
9
10 *J. Phys. Chem. A* **2014**, *118*, 5769-5778.

11
12
13
14 (20) Wang, Q. P.; Guo, X. X.; Wu, W. H.; Liu, S. X. Preparation of Fine Ag₂WO₄
15 Antibacterial Powders and Its Application in the Sanitary Ceramics. *Adv. Mater. Res.*, **2011**,
16
17 284-286, 1321-1325.

18
19
20
21
22
23 (21) Roca, R. A.; Sczancoski, J. C.; Nogueira, I. C.; Fabbro, M. T.; Alves, H. C.; Gracia, L.;
24 Santos, L. P. S.; de Sousa, C. P.; Andrés, J.; Luz, G. E.; et al. Facet-Dependent Photocatalytic
25 and Antibacterial Properties of α -Ag₂WO₄ Crystals: Combining Experimental Data and
26
27
28
29
30
31
32
33
34
35
36
37
38
39
40
41
42
43
44
45
46
47
48
49
50
51
52
53
54
55
56
57
58
59
60
Theoretical Insights. *Catal. Sci. Technol.* **2015**, *5*, 4091-4107.

(22) Longo, E.; Cavalcante, L. S.; Volanti, D. P.; Gouveia, A. F.; Longo, V. M.; Varela, J.
A.; Orlandi, M. O.; Andres, J. Direct in situ Observation of the Electron-driven Synthesis of
Ag Filaments on Alpha-Ag₂WO₄ Crystals. *Sci. Rep.* **2013**, *3*, 1676.

(23) Andres, J.; Gracia, L.; Gonzalez-Navarrete, P.; Longo, V. M.; Avansi, W., Jr.; Volanti,
D. P.; Ferrer, M. M.; Lemos, P. S.; La Porta, F. A.; Hernandez, A. C.; et al. Structural and
Electronic Analysis of the Atomic Scale Nucleation of Ag on alpha-Ag₂WO₄ Induced by
Electron Irradiation. *Sci. Rep.* **2014**, *4*, 5391.

1
2
3 (24) Pereira, W. d. S.; Andrés, J.; Gracia, L.; San-Miguel, M. A.; da Silva, E. Z.; Longo, E.;
4
5 Longo, V. M. Elucidating the Real-time Ag Nanoparticle Growth on α -Ag₂WO₄ During
6
7 Electron Beam Irradiation: Experimental Evidence and Theoretical Insights. *Phys. Chem.*
8
9 *Chem. Phys.* **2015**, *17*, 5352-5359.

10
11
12
13
14 (25) Longo, E.; Volanti, D. P.; Longo, V. M.; Gracia, L.; Nogueira, I. C.; Almeida, M. A. P.;
15
16 Pinheiro, A. N.; Ferrer, M. M.; Cavalcante, L. S.; Andrés, J. Toward an Understanding of the
17
18 Growth of Ag Filaments on α -Ag₂WO₄ and their Photoluminescent Properties: A Combined
19
20 Experimental and Theoretical Study. *J.Phys. Chem.C* **2014**, *118*, 1229-1239.

21
22
23
24
25 (26) San-Miguel, M. A.; da Silva, E. Z.; Zannetti, S. M.; Cilense, M.; Fabbro, M. T.; Gracia,
26
27 L.; Andres, J.; Longo, E. In situ Growth of Ag Nanoparticles on alpha-Ag₂WO₄ under
28
29 Electron Irradiation: Probing the Physical Principles. *Nanotechnol.* **2016**, *27*, 225703.

30
31
32
33
34 (27) Longo, E.; Avansi, W., Jr.; Bettini, J.; Andres, J.; Gracia, L. In situ Transmission
35
36 Electron Microscopy Observation of Ag Nanocrystal Evolution by Surfactant Free Electron-
37
38 driven Synthesis. *Sci. Rep.* **2016**, *6*, 21498.

39
40
41
42
43 (28) Roca, R. A.; Gouveia, A. F.; Lemos, P. S.; Gracia, L.; Andrés, J.; Longo, E. Formation
44
45 of Ag Nanoparticles on β -Ag₂WO₄ through Electron Beam Irradiation: A Synergetic
46
47 Computational and Experimental Study. *Inorg.Chem.* **2016**, *55*, 8661-8671.
48
49
50
51
52
53
54
55
56
57
58
59
60

1
2
3 (29) Roca, R. A.; Lemos, P. S.; Gracia, L.; Andrés, J.; Longo, E. Uncovering the Metastable
4 γ -Ag₂WO₄ Phase: a Joint Experimental and Theoretical Study. *RSC Advances* **2017**, *7*, 5610-
5 5620.
6
7
8

9
10
11 (30) Fabbro, M. T.; Gracia, L.; Silva, G. S.; Santos, L. P. S.; Andrés, J.; Cordoncillo, E.;
12 Longo, E. Understanding the Formation and Growth of Ag Nanoparticles on Silver Chromate
13 Induced by Electron Irradiation in Electron Microscope: A Combined Experimental and
14 Theoretical Study. *J. Solid State Chem.* **2016**, *239*, 220-227.
15
16
17
18
19

20
21 (31) Fabbro, M. T.; Saliby, C.; Rios, L. R.; La Porta, F. A.; Gracia, L.; Li, M. S.; Andres, J.;
22 Santos, L. P.; Longo, E. Identifying and Rationalizing the Morphological, Structural, and
23 Optical Properties of β -Ag₂MoO₄ Microcrystals, and the Formation Process of Ag
24 Nanoparticles on their Surfaces: Combining Experimental Data and First-Principles
25 Calculations. *Sci. Technol. Adv. Mater.* **2015**, *16*, 065002.
26
27
28
29
30
31
32
33
34
35

36
37 (32) de Oliveira, R. C.; Assis, M.; Teixeira, M. M.; da Silva, M. D. P.; Li, M. S.; Andres, J.;
38 Gracia, L.; Longo, E. An Experimental and Computational Study of β -AgVO₃: Optical
39 Properties and Formation of Ag Nanoparticles. *J. Phys. Chem. C* **2016**, *120*, 12254-12264.
40
41
42
43
44

45
46 (33) Botelho, G.; Sczancoski, J. C.; Andres, J.; Gracia, L.; Longo, E. Experimental and
47 Theoretical Study on the Structure, Optical Properties, and Growth of Metallic Silver
48 Nanostructures in Ag₃PO₄. *J. Phys. Chem. C* **2015**, *119*, 6293-6306.
49
50
51
52
53

1
2
3 (34) Ghatak, J.; Guan, W.; Mobus, G. In Situ TEM Observation of Lithium Nanoparticle
4 Growth and Morphological Cycling. *Nanoscale* **2012**, *4*, 1754-1759.
5
6
7

8
9
10 (35) Ito, Y.; Jain, H.; Williams, D. B. Electron-Beam Induced Growth of Cu Nanoparticles
11 in Silica Glass Matrix. *Appl. Phys. Lett.* **1999**, *75*, 3793-3795.
12
13
14

15
16
17 (36) Yang, Z.; Walls, M.; Lisiecki, I.; Pileni, M.-P. Unusual Effect of an Electron Beam on
18 the Formation of Core/Shell (Co/CoO) Nanoparticles Differing by Their Crystalline
19 Structures. *Chemistry of Materials* **2013**, *25*, 2372-2377.
20
21
22
23

24
25
26 (37) Hermannsdorfer, J.; de Jonge, N.; Verch, A., Electron Beam Induced Chemistry of Gold
27 Nanoparticles in Saline Solution. *Chem. Commun.* **2015**, *51*, 16393-16396.
28
29
30

31
32
33 (38). Assis, M. C., E.; Torres-Mendita, R.; Beltrán-Mir, H.; Mingués-Vega, G.; Fernandes,
34 A. G.; Leite, E. R.; Andrés, J.; Longo, E. Laser Induced Formation of Bismuth Nanoparticles.
35 *Phys. Chem. Chem. Phys.* **2018**, *20*, 13693-13696.
36
37
38
39

40
41
42 (39) Sepulveda-Guzman, S.; Elizondo-Villarreal, N.; Ferrer, D.; Torres-Castro, A.; Gao, X.;
43 Zhou, J. P.; Jose-Yacaman, M. In situ Formation of Bismuth Nanoparticles Through
44 Electron-beam Irradiation in a Transmission Electron Microscope. *Nanotechnol.* **2007**, *18*,
45 335604.
46
47
48
49

50
51
52 (40) Liu, L.; Wang, H.; Yi, Z.; Deng, Q.; Lin, Z.; Zhang, X. In situ Investigation of Bismuth
53 Nanoparticles Formation by Transmission Electron Microscope. *Micron* **2018**, *105*, 30-34.
54
55
56
57

1
2
3
4
5 (41) Li, J.; Chen, J.; Wang, H.; Chen, N.; Wang, Z.; Guo, L.; Deepak, F. L. In Situ Atomic-
6 Scale Study of Particle-Mediated Nucleation and Growth in Amorphous Bismuth to
7 Nanocrystal Phase Transformation. *Adv. Sci.* **2018**, *5*, 1700992.

8
9
10
11
12
13
14 (42) Flores-Castañeda, M.; Camps, E.; Camacho-López, M.; Muhl, S.; García, E.; Figueroa,
15 M. Bismuth Nanoparticles Synthesized by Laser Ablation in Lubricant Oils for Tribological
16 Tests. *J. Alloys Compd.* **2015**, *643*, S67-S70.

17
18
19
20
21
22
23 (43) Torrisi, L.; Silipigni, L.; Restuccia, N.; Cuzzocrea, S.; Cutroneo, M.; Barreca, F.; Fazio,
24 B.; Di Marco, G.; Guglielmino, S. Laser-Generated Bismuth Nanoparticles for Applications
25 in Imaging and Radiotherapy. *J. Phys. Chem. Solids* **2018**, *119*, 62-70.

26
27
28
29
30
31
32 (44) Escobar-Alarcón, L. G.; Velarde-Granados, E.; Sanchez, D. V.; Olea-Mejía, O.; Haro-
33 Poniatowski, E.; Castañeda, A. A.; Solis, D. Bismuth and Gold Nanoparticles Prepared by
34 Laser Ablation in Aqueous Solutions. *Advanced Materials Research* **2014**, *976*, 196-201.

35
36
37
38 (45) Kresse, G.; Hafner, J. *Ab Initio* Molecular-Dynamics Simulation of the Liquid-Metal-
39 Amorphous-Semiconductor Transition in Germanium. *Phys. Rev. B* **1994**, *49*, 14251-14269.

40
41
42
43 (46) Perdew, J. P.; Burke, K.; Ernzerhof, M. Generalized Gradient Approximation Made
44 Simple. *Phys. Rev. Lett.* **1996**, *77*, 3865-3868.

1
2
3 (47) Kresse, G. J., D. From Ultrasoft Pseudopotentials to The Projector Augmented-wave
4 Method. *Phys. Rev. B* **1999**, *59*, 1759-1775.
5
6
7

8
9
10 (48) Dudarev, S. L.; Botton, G. A.; Savrasov, S. Y.; Humphreys, C. J.; Sutton, A. P. Electron-
11 Energy-Loss Spectra and the Structural Stability of Nickel Oxide: An LSDA + U Study.
12 *Phys. Rev. B* **1998**, *57*, 1505-1509.
13
14
15
16
17

18
19 (49) Bader, R. F. W. *Atoms in Molecules: A Quantum Theory*; Oxford University Press:
20 Oxford, 1990.
21
22
23
24
25

26 (50) Matta, C. F.; Boyd, R. J. *An Introduction to the Quantum Theory of Atoms in Molecules.*
27 *In The Quantum Theory of Atoms and Molecules: From Solid State to DNA and Drug Design*;
28 Wiley-VCH Verlag GmbH & Co. KGaA: Weinheim, 2007.
29
30
31
32
33
34

35 (51) Popelier, P. L. A.; Aicken, F. M.; O'Brien, S. E. *Chemical Modelling: Applications and*
36 *Theory*; RCS: London, 2000.
37
38
39

40 (52) Andres, J.; Gracia, L.; Gouveia, A. F.; Ferrer, M. M.; Longo, E. Effects of Surface
41 Stability on the Morphological Transformation of Metals and Metal Oxides as Investigated
42 by First-Principles Calculations. *Nanotechnol.* **2015**, *26*, 405703.
43
44
45
46
47
48

49 (53) Botelho, G.; Sczancoski, J. C.; Andres, J.; Gracia, L.; Longo, E. Experimental and
50 Theoretical Study on the Structure, Optical Properties, and Growth of Metallic Silver
51 Nanostructures in Ag₃PO₄. *J. Phys. Chem. C* **2015**, *119*, 6293-6306.
52
53
54
55
56
57

1
2
3
4
5 (54) Liu, J.; Chen, S.; Liu, Q.; Zhu, Y.; Zhang, J. Correlation of Crystal Structures and
6 Electronic Structures with Visible Light Photocatalytic Properties of NaBiO₃. *Chem. Phys.*
7 *Lett.* **2013**, *572*, 101-105.
8
9
10

11
12
13
14 (55) Kumada, N.; Kinomura, N.; Seight, A. W. Neutron Powder Diffraction Refinement of
15 Ilmenite type Bismuth Oxides: ABiO₃ (A = Na, Ag). *Mater. Res. Bull.* **2000**, *35*, 2397-2402.
16
17
18

19
20
21 (56) B. Aurivillius. X-Ray Studies on Sodium Methabismuthate. *Acta Chem. Scand.*, **1955**,
22 *9*, 1219-1221.
23
24
25

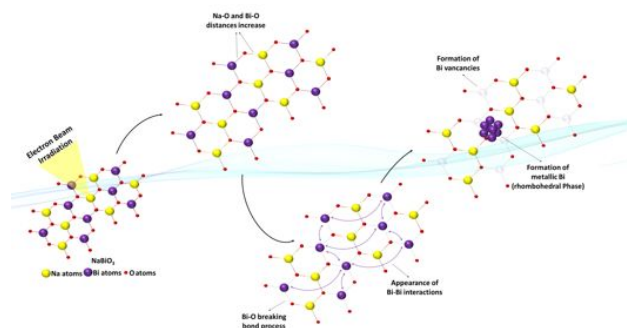
26
27
28 (57) Sillén, L. G. X-Ray Studies on Bismuth Trioxide. *Ark. Kemi. Mineral. Geol.*, **1937**, *12A*,
29 *1-15*.
30
31
32

33
34
35 (58) Irmawati, R.; Noorfarizan Nasriah, M. N.; Taufiq-Yap, Y. H.; Abdul Hamid, S. B.
36 Characterization of Bismuth Oxide Catalysts Prepared from Bismuth Trinitrate Pentahydrate:
37 Influence of Bismuth Concentration. *Catal. Today* **2004**, *93-95*, 701-709.
38
39
40
41

42
43
44 (59) Niu, K.-Y.; Liao, H.-G.; Zheng, H. Visualization of the Coalescence of Bismuth
45 Nanoparticles. *Microsc. Microanal.* **2014**, *20*, 416-424.
46
47
48

49
50
51 (60) Sailer, R.; McCarthy, G. North Dakota State University, Fargo, North Dakota, USA,
52 ICDD Grant-in-Aid, 1992.
53
54
55

TOC Graphic



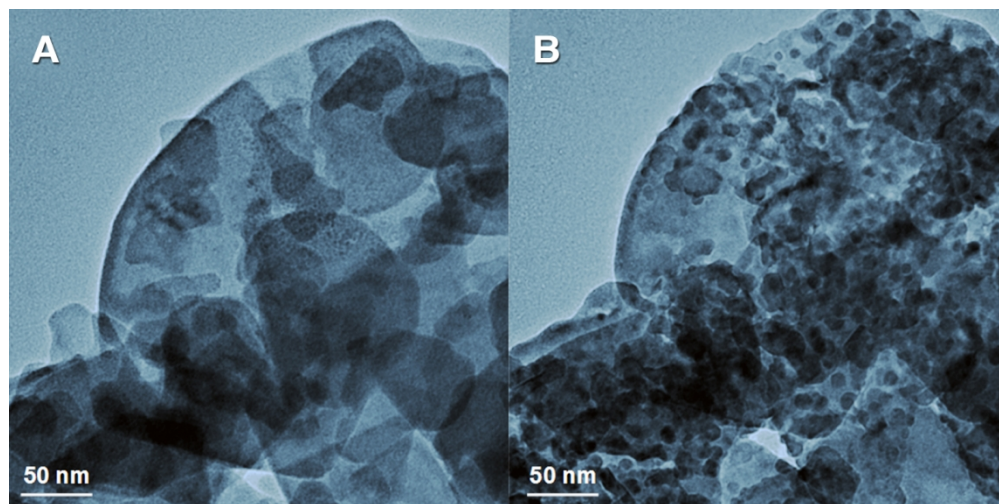


Figure 1: (A) Low-magnification TEM image of the sample before the irradiation by electron beam and (B) after 10 minutes of exposure to irradiation by electron beam.

136x68mm (300 x 300 DPI)

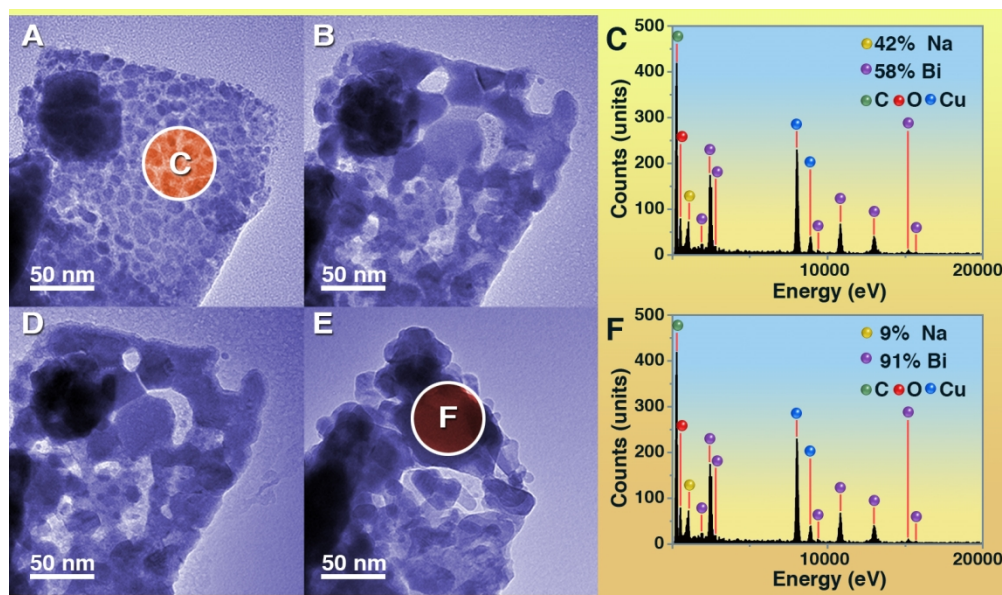


Figure 2: TEM image of the sample after (A) 10, (B) 15, (D) 20 and (E) 30 minutes of exposure. (C) and (F) EDS of the white circle in the image and their quantification.

136x81mm (300 x 300 DPI)

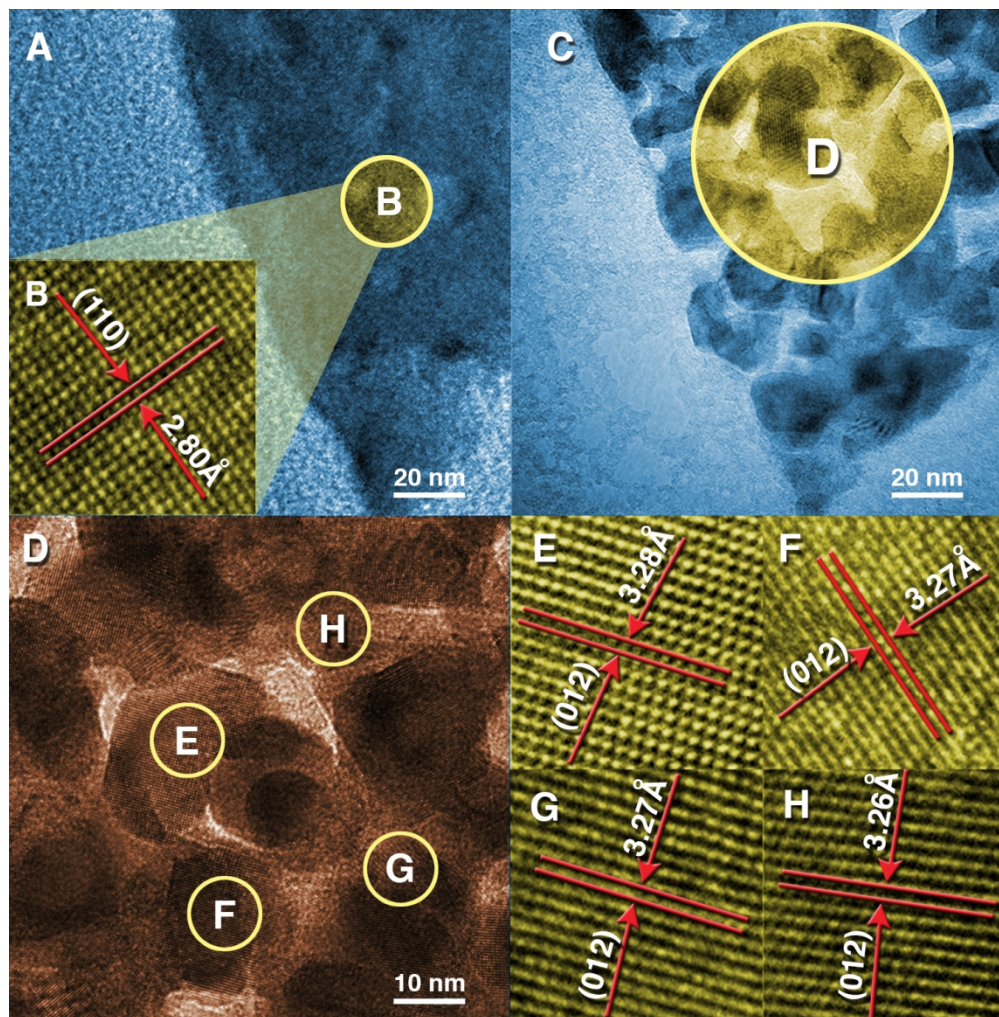


Figure 3 - TEM image of the NaBiO₃ before (A-B) the irradiation by electron beam and after (C). (D) HR-TEM micrographs at higher magnification (C). (E), (F), (G) and (H) NPs of Bi rhombohedral.

127x128mm (300 x 300 DPI)

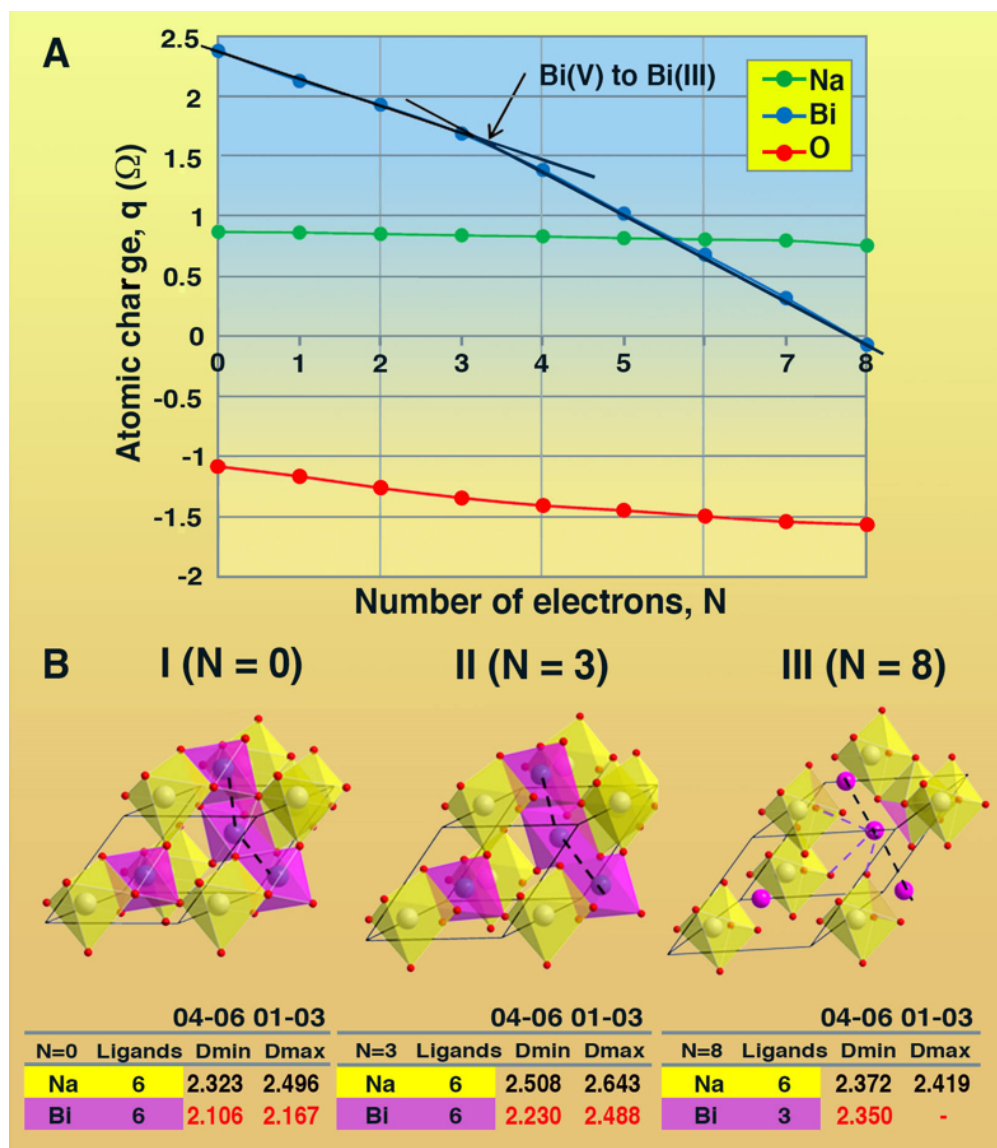


Figure 4 - (A) Bader charge density of Bi, Na and O centers as a function of the number of electrons added. $q(\Omega)$ represents the number of valence electrons minus the calculated charge density; (B) Primitive cell without (I) and with the addition of 3 (II) and 8 electrons (III) in NaBiO_3 and the minimum and maximum distances in Å (dmin and dmax, respectively) of the metallic centers to their oxygen atoms.

133x151mm (150 x 150 DPI)

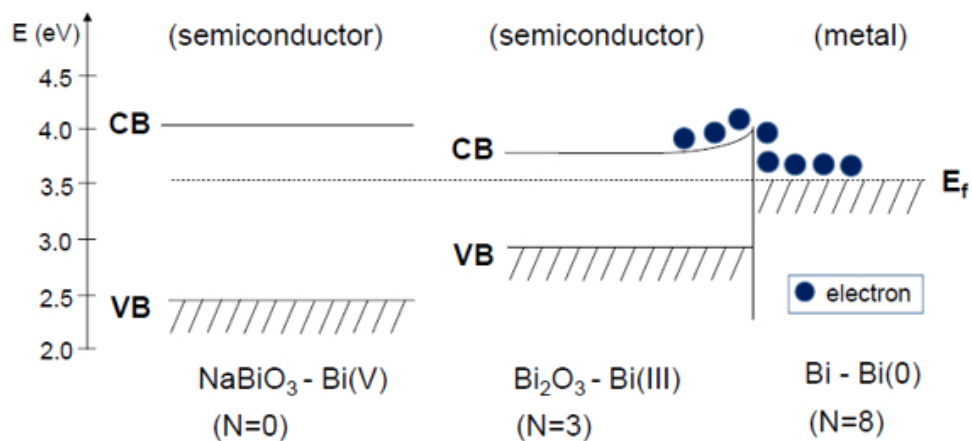


Figure 5 - Variation of the positions of VB and CB as a function of the number of electrons added, N . The position of the Fermi energy level, E_f , is placed once the metallic Bi is formed.

99x45mm (150 x 150 DPI)

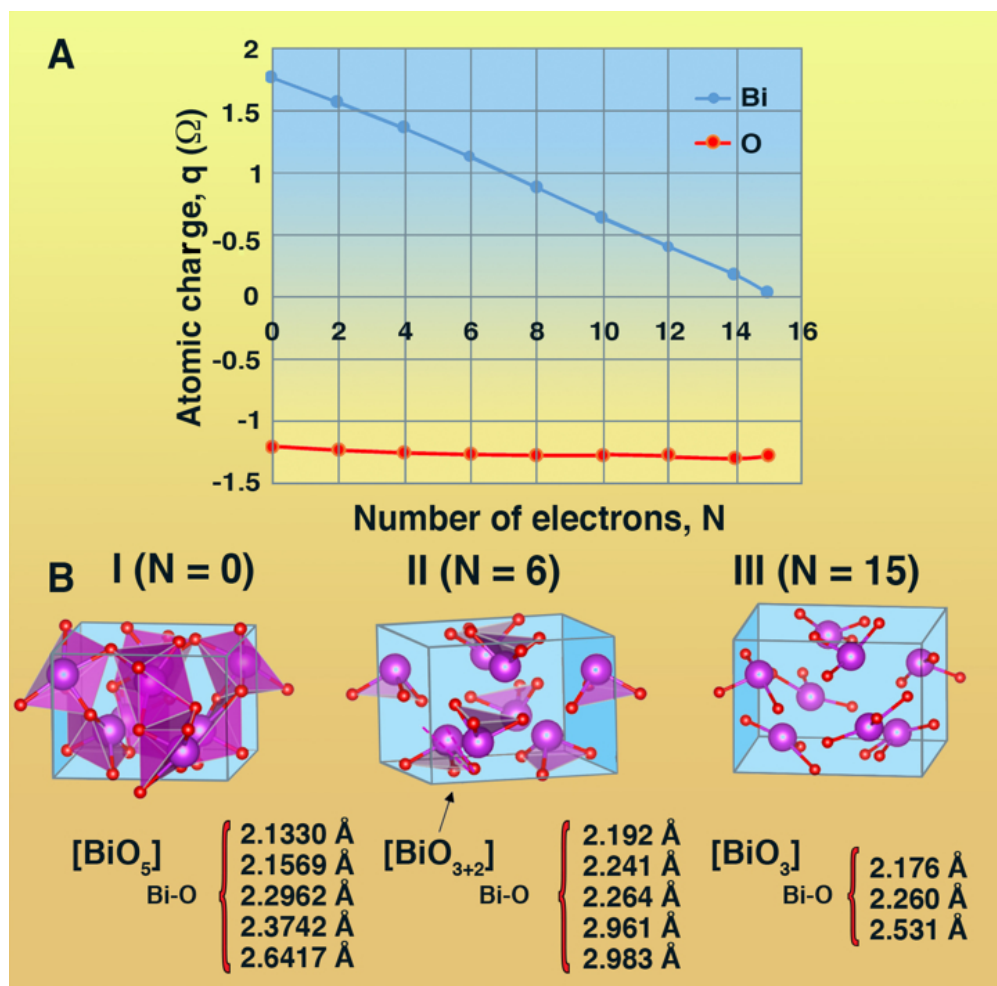
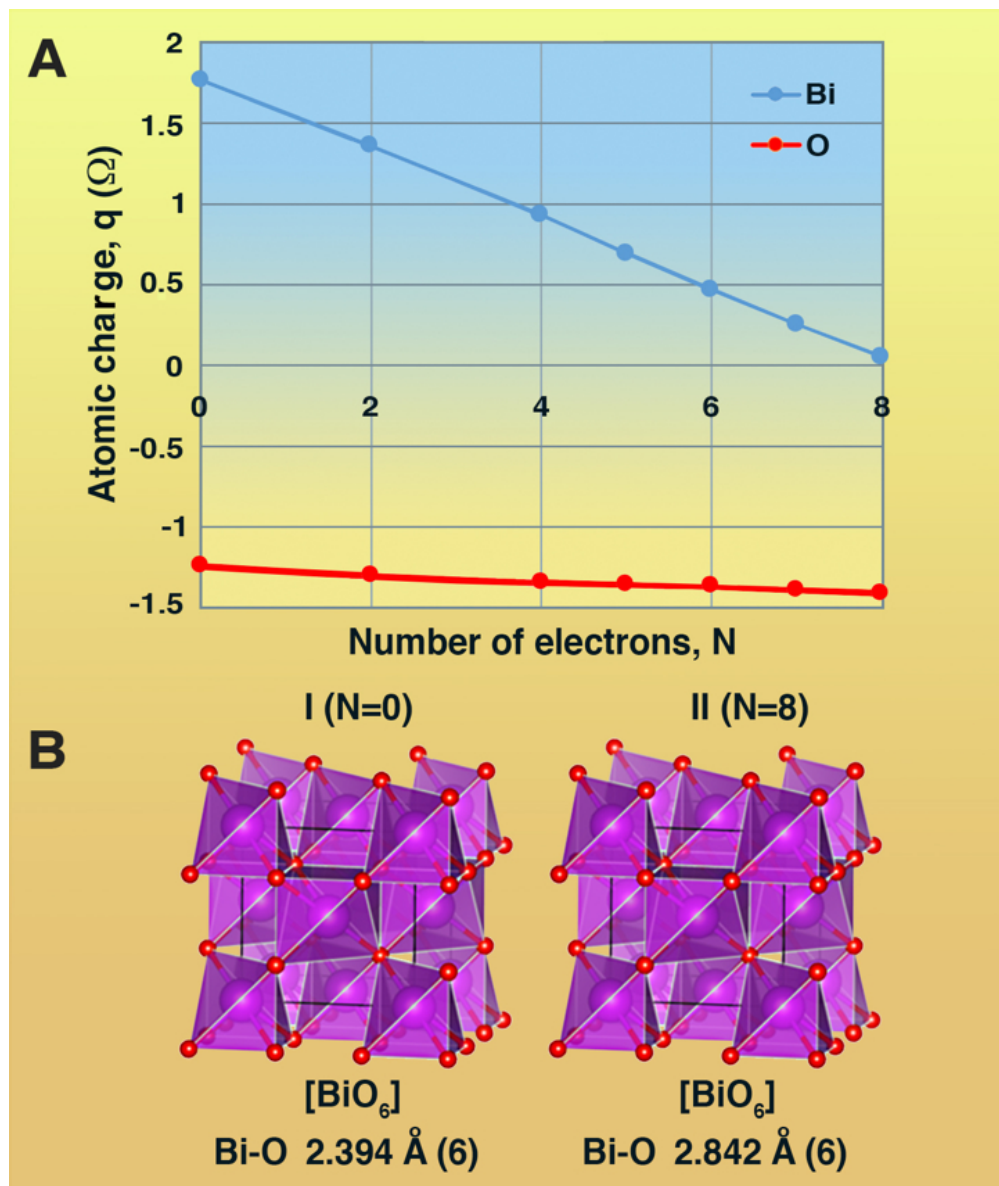


Figure 6 - (A) Bader charge density of Bi and O centers as a function of the number of electrons added. (B) Unit cell β -Bi₂O₃ without (I), with the addition of 6 electrons (II) and with the addition of 15 electrons (III); and the Bi-O distances of the structural clusters.

122x120mm (150 x 150 DPI)



122x144mm (150 x 150 DPI)

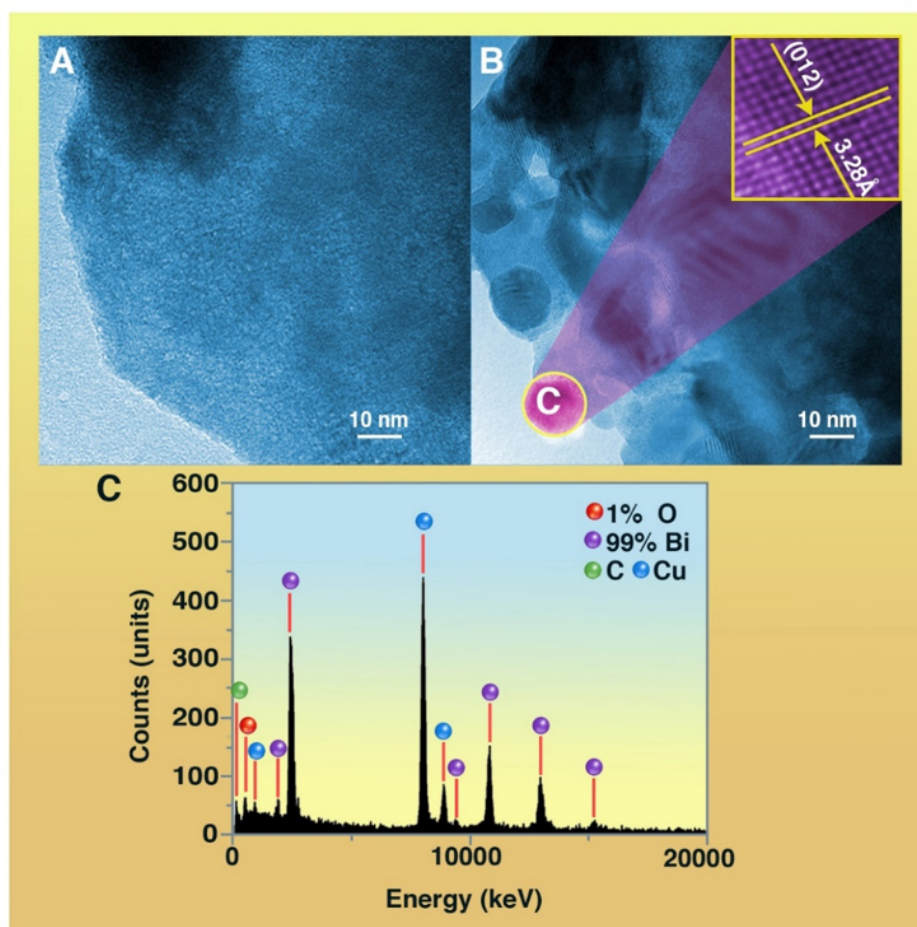


Figure 8 - (A) TEM image of the β - Bi_2O_3 before the irradiation by electron beam and (B) after 15 minutes exposure. (C) EDS of the yellow circle in the image and their quantification.

133x132mm (150 x 150 DPI)

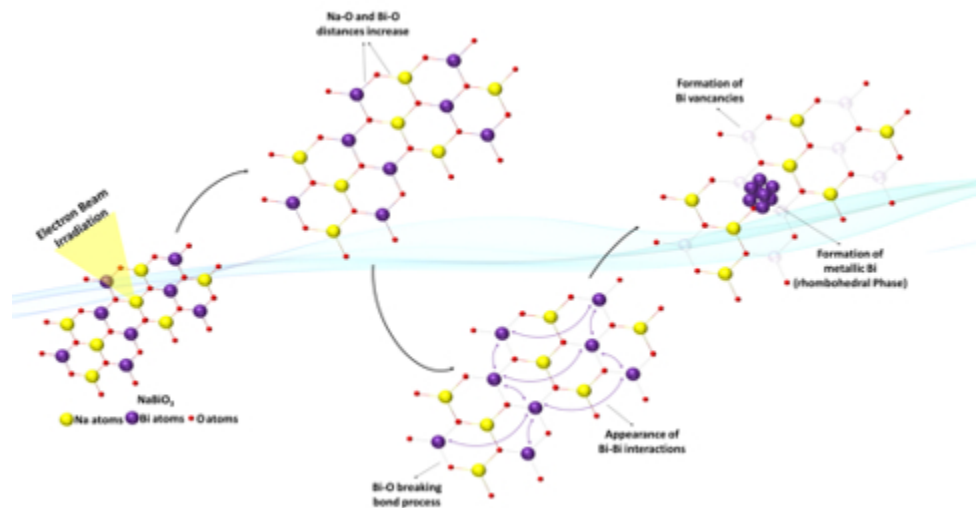
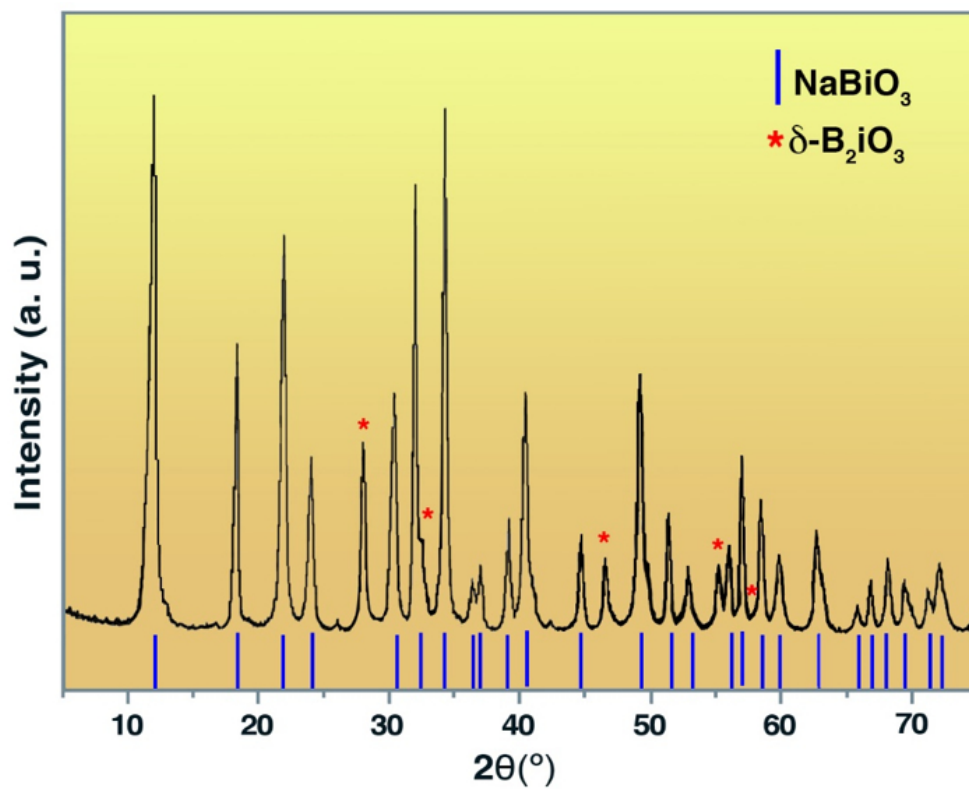
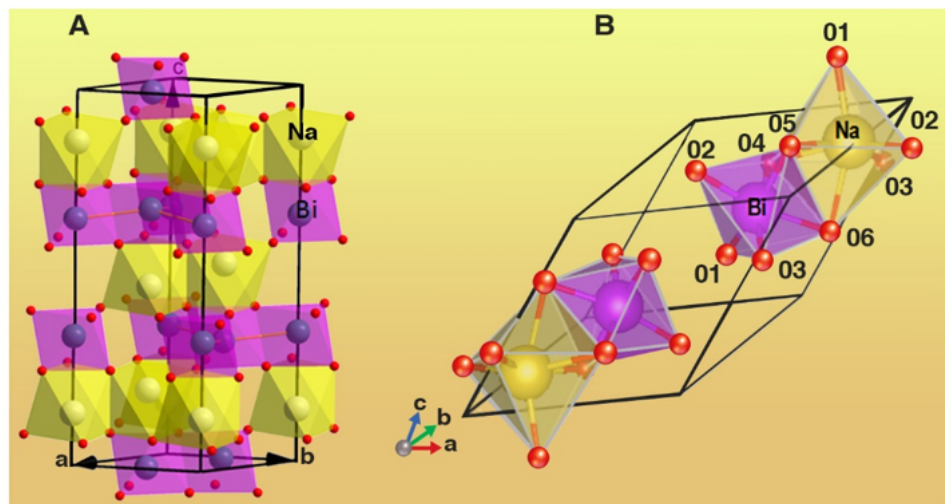


Table of Contents (TOC) Image

82x45mm (150 x 150 DPI)

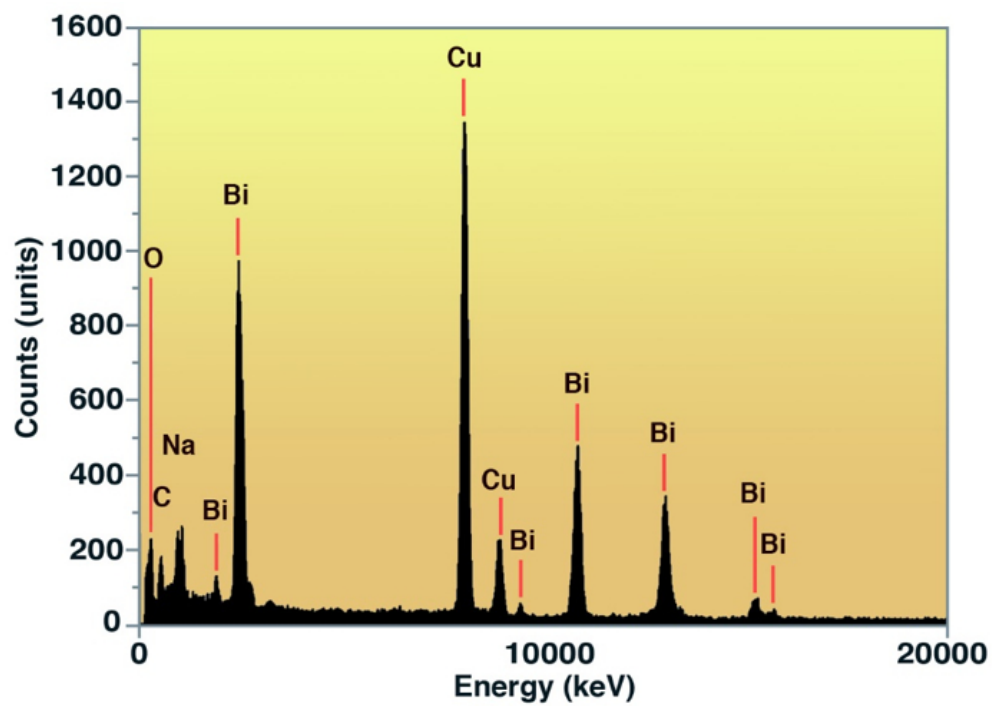
XRD patterns for commercial NaBiO₃.

121x96mm (150 x 150 DPI)



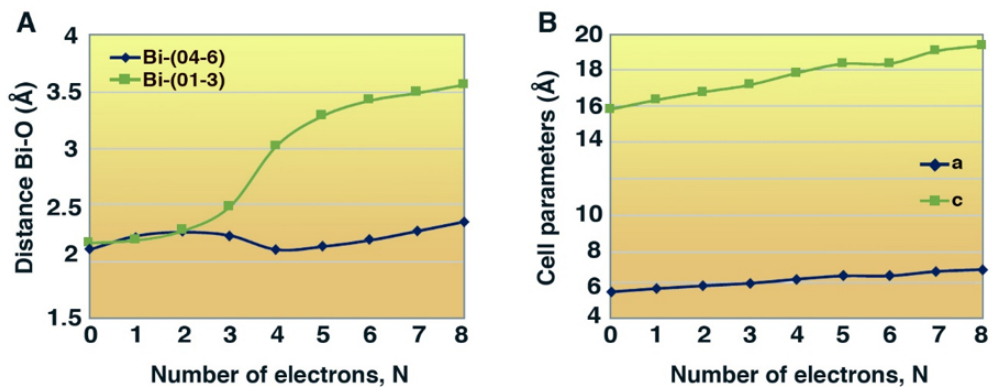
Conventional (A) and primitive cell (B) of NaBiO₃ in the rhombohedral space group R-3

126x65mm (150 x 150 DPI)



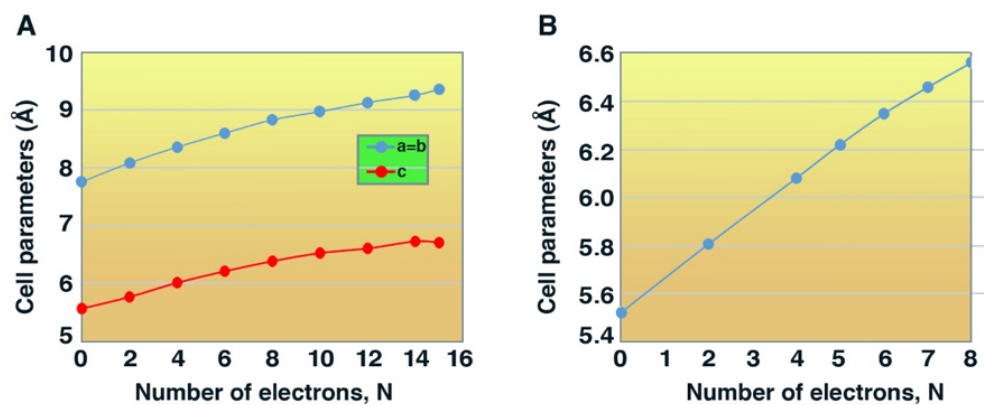
EDS analysis of NaBiO₃.

118x84mm (150 x 150 DPI)



(A) Variation of Bi-O distances (B) and of cell parameters in NaBiO₃ structure as a function of the number of electrons added, N.

154x63mm (150 x 150 DPI)



Variation of cell parameters in Bi₂O₃ structure as a function of the number of electrons added, N . (A) β -Bi₂O₃ and (B) δ -Bi₂O₃.

151x70mm (150 x 150 DPI)